JOURNAL OF MATERIALS SCIENCE 21 (1986) 2843–2849

Dislocation structures in Zr_3Al-based alloys

P. HOLDWAY, A. E. STATON-BEVAN
Department of Metallurgy and Materials Science, Imperial College, London SW7 2BP, UK

Transmission electron microscopy has been used to investigate dislocation structures in deformed binary and ternary Zr_3Al-based alloys. In the binary alloy deformed at temperatures between 293 and 673 K the dislocations in the Zr_3Al phase consisted of $a/3\langle 1\,1\,2\rangle$-type partial dislocations bounding superlattice intrinsic stacking fault on $\{1\,1\,1\}$ planes. The $\{1\,1\,1\}$ $a/3\langle 1\,1\,\bar{2}\rangle$ stacking fault energy was approximately 2 mJ m^{-2} at 673 K. In binary specimens deformed between 873 and 1073 K cube slip predominated. Dislocations consisted mainly of $a/2\langle 1\,1\,0\rangle$ pairs separated by antiphase boundary. For this temperature range the $\{1\,0\,0\}$ $a/2\langle 0\,1\,1\rangle$ antiphase boundary energy was between 30 and 45 mJ m^{-2}. Alloying with niobium or titanium was found to increase the $\{1\,1\,1\}$ $a/3\langle 1\,1\,\bar{2}\rangle$ stacking fault energy and thus increase the propensity for antiphase boundary-type dissociation.

1. Introduction

1.1. Background

Alloys based on the $L1_2$ intermetallic compound Zr_3Al have been under investigation as potential structural materials for fuel sheaths or pressure tubes in nuclear reactors [1]. From a theoretical point of view the mechanical properties of Zr_3Al based alloys are of interest because, like several $L1_2$ materials, e.g. Ni_3Al and Ni_3Ga, they exhibit an anamolous temperature dependence of the flow stress. Schulson and Roy [2] have reported an increase in the flow stress with increasing temperature between 350 and 900 K for binary alloys having a Zr_3Al grain size greater than approximately 2 μm.

1.2. Slip systems and dislocation structures in $L1_2$ crystals

Two types of primary slip system are found to operate in $L1_2$ crystals: $\{1\,1\,1\}\langle 1\,\bar{1}\,0\rangle$ and $\{0\,0\,1\}\langle 1\,1\,0\rangle$.

All $L1_2$ materials exhibit octahedral slip, normally accompanied by a tendency for screw dislocation segments to cross-slip onto cube planes by the so-called "Kear–Wilsdorf" mechanism [3]. The driving force for cross-slip is the low cube plane antiphase boundary (APB) energy of the $L1_2$ structure [4].

The total superlattice dislocation Burgers vector in $L1_2$ crystals is $a\langle 1\,1\,0\rangle$, where a is the lattice parameter. For octahedral slip two types of dissociation have been observed [5] and these are shown diagramatically in Fig. 1. In dissociation Scheme I, Fig. 1a, two $a/2\langle 1\,1\,0\rangle$ dislocations are separated by a region of APB. In Scheme II, Fig. 1b, two $a/3\langle 1\,1\,2\rangle$-type partials are separated by a region of superlattice intrinsic stacking fault (S-ISF) on a $\{1\,1\,1\}$ plane. For cube slip only $a/2\langle 1\,1\,0\rangle$ pairs are observed.

1.3. Transmission electron microscopy studies

A previous transmission electron microscopy (TEM) study was carried out on binary Zr_3Al-based specimens deformed at room temperature [6]. Evidence was found of $\{1\,1\,1\}\langle 1\,1\,0\rangle$ slip and S-ISF-type dislocation dissociation but not of primary $\{0\,0\,1\}\langle 1\,1\,0\rangle$ slip or APB-type dissociation.

The present study investigated binary and ternary specimens deformed at various temperatures in the range 293 to 1073 K. Of particular interest was the possibility of primary cube slip and APB-type dislocation dissociation.

2. Experimental procedure

2.1. Materials

Slabs of Zr–8.6 wt % Al, which had been hot rolled at 1373 K were used as a basis for the alloys investigated in this study. Ternary alloys were produced by remelting the binary alloy with the required amounts of zirconium, aluminium, niobium and titanium in an arc furnace. Heat treatment was carried out at 1160 K resulting in microstructures consisting of Zr_3Al, α-Zr and Zr_2Al, see Table I.

2.2. Mechanical testing

Compression specimens 3 mm × 3 mm × 10 mm were cut from the hot rolled alloy B and heat treated. Round tensile specimens of alloys N1 and T2, having a 4.5 mm diameter and a 16 mm gauge length, were machined from heat treated ingots. Prior to testing these specimens were annealed for 1 h at 1160 K and then electropolished.

2.3. Transmission electron microscopy

Discs 3 mm in diameter were spark machined from slices cut at 45° to the stress axis from the central portions of the test specimens. Thin foils were produced by jet electropolishing in a solution of 5% perchloric acid in ethanol at 30 V and at ~240 K. Burgers vector and stacking fault analysis was achieved by setting up strong two-beam conditions with S, the deviation from the Bragg angle, zero or slightly positive.

0022–2461/86 $03.00 + .12

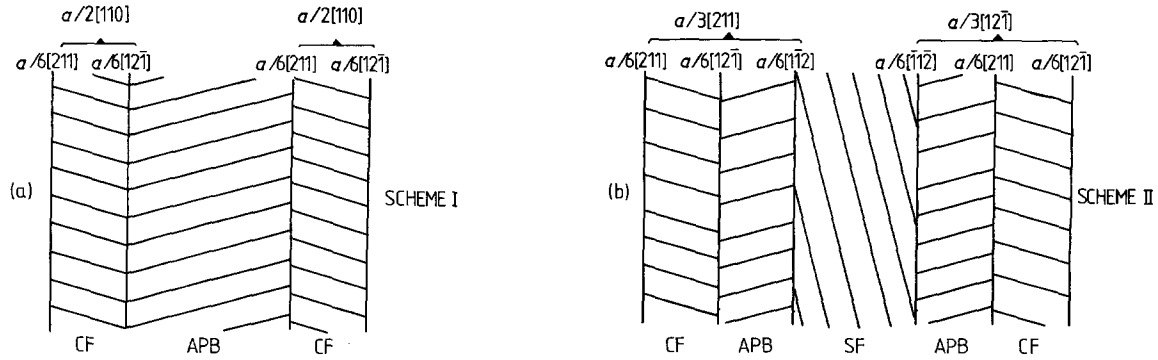

Figure 1 Two possible dissociation modes for a superlattice dislocation of total Burgers vector $a[1\,1\,0]$ on the $(\bar{1}\,1\,1)$ plane in the $L1_2$ crystal structure, see text. APB = antiphase boundary, SF = stacking fault, CF = complex fault.

3. Results and discussion

3.1. Dislocation structures in binary alloy B, deformed in compression at temperatures in the range 293 to 673 K

3.1.1. S-ISF dislocations

Examples of the dislocation structures in specimens deformed at room temperature and 673 K are shown in Figs 2 and 3, respectively. Widely separated S-ISF dislocations (Scheme II, Fig. 1b) were the predominant type observed over the whole of this temperature range.

3.1.2. Stacking fault vectors

In all cases the stacking faults were found to be intrinsic and to have fault vectors of the type $R = 1/3\langle 1\,1\,1\rangle$, as has been observed previously for lightly deformed Zr_3Al [6] and for the $L1_2$ compounds Ni_3Al [7] and Ni_3Ga [8]. For example, the faults such as 1,2 3,4 and 5,6 in Fig. 3 were visible for $\boldsymbol{g} = 2\,0\,0$, $0\,2\,0$ and $2\,2\,0$ but invisible for $\boldsymbol{g} = \bar{2}\,2\,0$ (Fig. 3c) indicating fault vectors of the type $R = \pm 1/3[1\,1\,1]$ or $\pm 1/3[1\,1\,\bar{1}]$. The top dark fringe in the bright field image, e.g. at × in Fig 3a, becomes bright in the high resolution dark field (HRDF) image using the negative $\boldsymbol{g}$ vector (Fig. 3b). This indicates that it marks the intersection of the fault with the top of the foil. Thus, taking into account the nature of the edge fringe contrast the fault vector $R = 1/3[1\,1\,1]$. The intrinsic nature of the faults was determined using the criterion that, allowing for image rotation, the $\boldsymbol{g}$ vector in dark field pointed towards the bright outer fringe [9], see Fig 3b.

3.1.3. Stacking fault energy

Measurement of the separation of partial dislocations at 673 K gave a value for the stacking fault energy of approximately $2\,mJ\,m^{-2}$. This value is much lower than the room temperature value of $80\,mJ\,m^{-2}$ obtained by Howe *et al.* [6]. It is however similar to the value of $5\,mJ\,m^{-2}$ quoted for Ni_3Ga for temperatures at which S-ISF dislocations predominate [10], see Table II. It has been proposed [19] that for stacking fault dislocations to be stable the ratio

$$\frac{\{1\,1\,1\}\text{ APB energy}}{\{1\,1\,1\}\text{ SF energy}} \geqslant 25 \text{ to } 35$$

since in the temperature range under discussion stacking fault dislocations predominate, a SF energy of $2\,mJ\,m^{-2}$ (present study) would indicate an APB energy $\geqslant 500\,mJ\,m^{-2}$, whereas a SF energy of $80\,mJ\,m^{-2}$ [6] would indicate an APB energy $\geqslant 2000\,mJ\,m^{-2}$. From Table II it may be seen that the former value is more in line with those for other $L1_2$ materials.

3.1.4. The Burgers vectors of the partial dislocations bounding the stacking faults

The interpretation of the Burgers vectors of partial dislocations bounding the stacking faults is made difficult by the ambiguity of the contrast when $\boldsymbol{g}\cdot\boldsymbol{b} = \frac{2}{3}$ or $\pm\frac{4}{3}$ [9]. Thus only $\boldsymbol{g}$ vectors of the type $\langle 3\,1\,1\rangle$ and certain $\langle 2\,2\,0\rangle$ were found to give consistent results. Using the latter type of reflections, the Burgers vectors of dislocation pairs bounding stacking faults were found to be $a/3\langle 2\,1\,1\rangle$-type pairs, that is undissociated "Scheme II" in Fig. 1b. The contrast for dislocation pair 1,2 in Fig. 3, for example, corresponded to the Burgers vectors $\pm(a/3[\bar{2}\,1\,1]$, $a/3[\bar{1}\,2\,\bar{1}])$.

The dissociation of the $a/3\langle 2\,1\,1\rangle$ partials into 3 Schockley partials, as shown in Fig. 1b, is not thought to occur. Partial number 4 in Fig. 3, for example, which bounds S-ISF on $(1\,1\,1)$, is invisible for $\boldsymbol{g} = \bar{2}\,2\,0$ (Fig. 3c). The contrast for all possible dissociations into 3 Schockley patials, such as

$$\frac{a}{3}[1\,1\,\bar{2}] \rightarrow \frac{a}{6}[2\,\bar{1}\,\bar{1}] + \frac{a}{6}[\bar{1}\,2\,\bar{1}] + \frac{a}{6}[1\,1\,\bar{2}]$$

TABLE I Compositions, heat treatments and microstructures of the alloys investigated

Alloy code	Composition (wt %)				Heat treatment at 1160 K (h)	Volume fractions of phases (%)			Average grain size (μm)
	Zr	Al	Nb	Ti		α-Zr	Zr_2Al	Zr_3Al	
B	91.40	8.60	–	–	8	15 ± 6	11 ± 5	Balance	6
N1	90.18	8.60	1.22	–	9	19 ± 5	6 ± 5	Balance	4
T2	91.15	8.22	–	0.63	25	24 ± 5	6 ± 3	Balance	4

TABLE II Values of stacking fault energy and antiphase boundary energy in some $L1_2$ alloys

Material	$\{1\,1\,1\}\,a/2\langle 1\,1\,0\rangle$ APB energy ($mJ\,m^{-2}$)	$\{1\,0\,0\}\,a/2\langle 1\,1\,0\rangle$ APB energy ($mJ\,m^{-2}$)	$\{1\,1\,1\}\,a/3\langle 1\,1\,2\rangle$ SF energy ($mJ\,m^{-2}$)	Predominant dislocation type
Cu_3Au	30 [11] 39 ± 5 [12] 91 quoted by [13]	10 [11]	13 ± 1.5 [12]	APB at room temperature
Ni_3Al	180 ± 30 [14] 164 quoted by [15] 252 [13] 250 to 350 [18]	140 ± 14 [14] 47 to 64 [16] 82 ± 8 [17]* 94 ± 10 [17]†	10 ± 5 [14] 29 ± 5 [17]† 46 ± 6 [17]*	APB usually observed, but SF dislocations produced by multiple slip
Ni_3Ga	110 ± 30 [19]	17 ± 5 [19] 40 [8]	5 [10]	SF at low temperatures
Zr_3Al	Assumed to be higher than SF energy at room temperature due to the absence of APB dislocations	30 to 45 [present work, alloy B] above 873 K	70 to 90 [6] ~2 (alloy B) at 673 K [present work] ~9 (alloy N1) at 673 K	SF at room temperature

*22.9 at % Al.
†24 at % Al.

would render 2 Schockley partials visible and one invisible for this reflection. Partial 4 is thus considered to have the Burgers vectors $\pm a/3[1\,1\,\bar{2}]$.

For Ni_3Ga the predominant Burgers vectors have been reported to be $+\boldsymbol{b} - \boldsymbol{b}$ $a/3\langle 2\,1\,1\rangle$ pairs [10]. This was not found to be the case for Zr_3Al. The pair 3,4 in Fig. 3 have obviously not got antiparallel Burgers vectors since 3 is visible and 4 is invisible for $\boldsymbol{g} = \bar{2}\,2\,0$, Fig. 3c.

Dissociations of the type

$$\frac{a}{3}[\bar{1}\,\bar{1}\,2] \rightarrow \frac{a}{6}[1\,\bar{2}\,1] + \frac{a}{2}[\bar{1}\,0\,\bar{1}]$$

followed by cross-slip of the $a/2[\bar{1}\,0\,1]$ dislocation onto a cube plane have also been proposed for $L1_2$ crystals [7]. No evidence could be found of this type of dissociation from contrast experiments, in either binary or ternary specimens for any of the test temperatures.

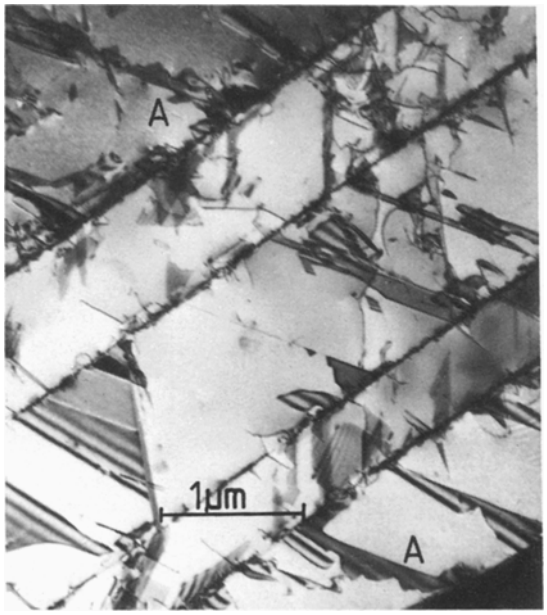

Figure 2 Bright-field transmission electron micrograph showing the dislocation structure observed in alloy B deformed 1.4% at 293 K. Note dislocations originating from twin boundaries in the Zr_3Al and 'sawtooth' stacking fault at A.

3.1.5. Sawtooth stacking faults

Several examples of "sawtooth' stacking faults were observed, e.g. at A in Figs 2 and 3. Similar faults have been observed in Ni_3Al [7] and Ni_3Ga [20]. Two different mechanisms have been proposed for their origin and these are illustrated schematically in Fig. 4.

In the first mechanism, Giamei *et al.* [7] have proposed that stacking faults originate for $a/3\langle 1\,1\,2\rangle$ superlattice pairs. The dislocation dissociations which result in the structure shown in Fig. 4a may be summarized as follows

$$a[1\,1\,0] \rightarrow \frac{a}{3}[2\,1\,1] + \frac{a}{3}[1\,2\,\bar{1}]$$

$$\frac{a}{3}[2\,1\,1] \rightarrow \frac{a}{6}[1\,\bar{1}\,2] + \frac{a}{2}[1\,1\,0]$$

separated by (0 0 1) APB

also

$$\frac{a}{3}[2\,1\,1] \rightarrow \frac{a}{6}[1\,2\,\bar{1}] + \frac{a}{2}[1\,0\,1]$$

separated by (0 1 0) APB

$$\frac{a}{3}[1\,2\,\bar{1}] \rightarrow \frac{a}{6}[2\,1\,1] + \frac{a}{2}[0\,1\,\bar{1}]$$

separated by (1 0 0) APB

Note the three different orientations of $\{1\,0\,0\}$ APB.

Recently Veyssière *et al.* [14] have proposed an alternative mechanism in which sawtooth faults are derived from $a/2[1\,1\,0]$ superlattice pairs. The dissociation reactions, which produce a single orientation of $\{1\,0\,0\}$ APB (see Fig. 4b), are as follows

$$a[0\,\bar{1}\,1] \rightarrow \frac{a}{2}[0\,\bar{1}\,1] + \frac{a}{2}[0\,\bar{1}\,1]$$

separated by (1 0 0) APB

$$\frac{a}{2}[0\,\bar{1}\,1] \rightarrow \frac{a}{6}[2\,1\,1] + \frac{a}{3}[\bar{1}\,\bar{2}\,1]$$

separated by $(\bar{1}\,1\,1)$ S-ISF

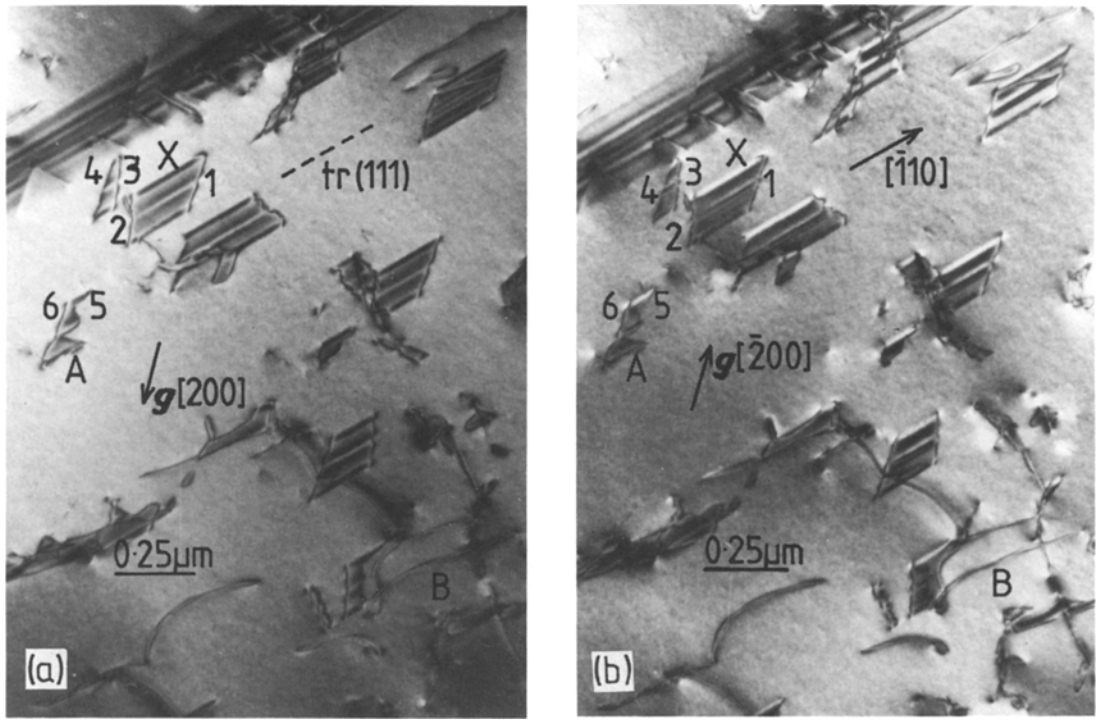

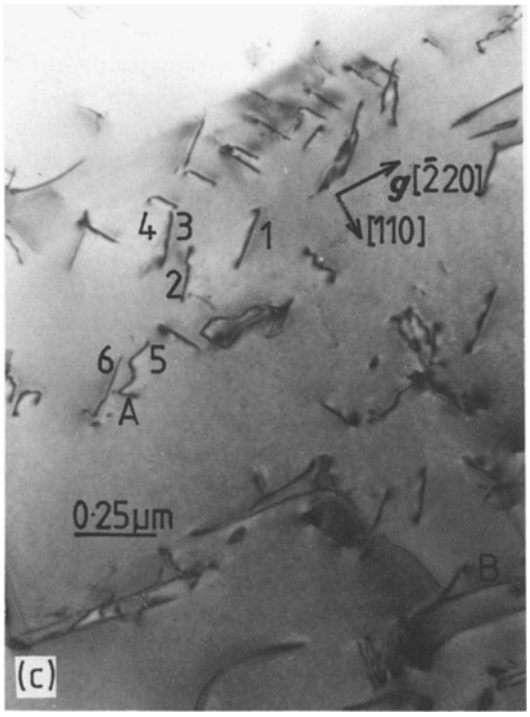

Figure 3 Stacking fault dislocations observed in Zr_3Al deformed $\approx$ 1% at 673 K. Beam direction [0 0 1]. (a) Bright-field $g = 2\,0\,0$; (b) HRDF $g = \bar{2}\,0\,0$; (c) bright-field $g = \bar{2}\,2\,0$.

Both of the proposed schemes (Figs 4a and b) require an $(a/2)\langle 1\,1\,0\rangle/(a/6)\langle 1\,1\,2\rangle$ pair, however as was mentioned in Section 3.1.4 no evidence was found of such pairs in the present study. Sawtooth stacking faults in Zr_3Al may therefore be bounded by undissociated $a/3\langle 1\,1\,2\rangle$-type partials, as shown in Fig. 4c.

3.1.6. APB dislocations

Although S-ISF type dislocations predominated over the temperature range 293 to 673 K, a few APB-type dislocations (Scheme I, Fig. 1a) were also observed. For example, $a/2[1\,\bar{1}\,0]$ pairs may be seen at B in Fig. 3.

3.2. Dislocations observed in binary alloy B, deformed in compression at temperatures in the range 873 to 1073 K

Dislocation structures in specimens deformed in this temperature range are shown in Figs 5 to 7. At these higher temperatures the predominant dislocation type was found to be APB separated $a/2\langle 1\,1\,0\rangle$ superlattice pairs, i.e. Scheme I, Fig. 1a.

At 873 K very few S-ISF dislocations were observed and the APB dislocations often formed dipoles on $\{1\,1\,1\}$ planes.

At 973 K almost no S-ISF dislocations were observed and the APB dislocations were found to lie on cube clip planes. This may be seen in Fig. 5, which shows a specimen which had been deformed 1.3% at 973 K. APB-type dislocations lie in the (0 0 1) plane of the foil and interaction with a second cube slip system has produced debris parallel to the trace of (1 0 0). Figs 6 and 7 show dislocation structures in specimens which were deformed at 1073 K. At this temperature also, APB-type dislocations were found to predominate. The dislocations tended to be confined to narrow slip bands (see Fig. 7) involving slip on one or more cube planes. These slip bands are thought to originate from stress concentrations at grain boundaries, resulting from grain boundary sliding which is known to occur at this temperature.

In Figs 6 and 7 there is much evidence of interaction between dislocations on different cube planes resulting in debris in the form of loops (e.g. at L in Fig. 6), dipoles and jogged dislocations. The alternate single and double images along the lengths of dislocations in Fig. 6 are thought to be due to the cross-slip of alternate segments from cube to octahedral planes. The single segments are parallel to the trace of $(1\,1\,\bar{1})$

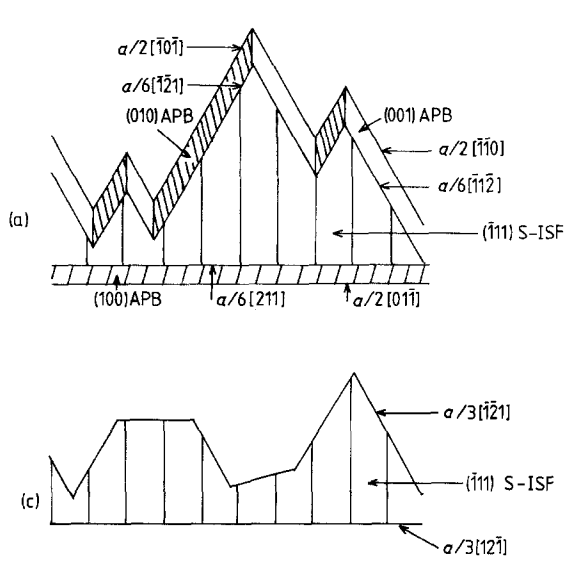

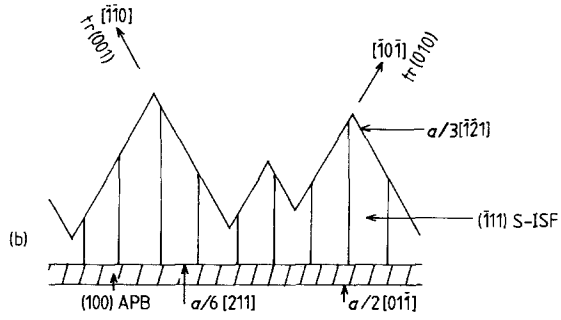

Figure 4 Schematic representations of a 'sawtooth' S-ISF on the $(\bar{1}\,1\,1)$ plane produced by (a) the dissociation of $a/3\langle 1\,1\,2\rangle$ superlattice pairs [7], (b) the dissociation of $a/2\langle 1\,1\,0\rangle$ superlattice pairs [14] and (c) undissociated $a/3\langle 1\,1\,2\rangle$ superlattice pairs, see text.

which is perpendicular to the plane of the foil. At higher temperatures therefore the APB dislocations are able to glide on cube planes, as a result of the relative lowering of the $\{1\,0\,0\}$ lattice friction stress and in addition may also cross-slip back onto octahedral planes. Measurements of the partial dislocation separations over the whole of this temperature range gave values for $\{1\,0\,0\}\,a/2\langle 0\,1\,1\rangle$ APB energy in the range 30 to 45 mJ m^{-2}.

3.3. Dislocation structures observed in ternary alloys T2 and N1 deformed in tension at 273 and 673 K

3.3.1. 273 K

The titanium alloy T2 was investigated at this temperature. The dislocation structure consisted of S-ISF separated $a/3\langle 1\,1\,2\rangle$-type partials (Fig. 8) as for the binary alloy deformed at the same temperature (Fig. 2). In both these alloys dislocations appeared to have nucleated from grain boundaries and twin boundaries.

3.3.2. 673 K

Both the titanium alloy T2 and the niobium alloy, N1, were tested at this temperature. In both alloys S-ISF and APB dislocations were found to coexist (see Fig. 9). This behaviour differs from that of the binary alloy in which S-ISF dislocations predominated at this temperature (Fig. 3). The APB dislocations were often observed to form screw dipoles (e.g. at T in Fig. 9), whilst the S-ISF dislocations sometimes formed loops or more complex phases (e.g. at A, B and C), often with bounding partials parallel to $\langle 1\,1\,0\rangle$ projections. Configurations such as those in Fig. 9 suggest that the S-ISF dislocations may have formed as a result of interactions between intersecting APB dislocations. It was not possible to find a dissociation scheme to explain the contrast from these bounding partials. In

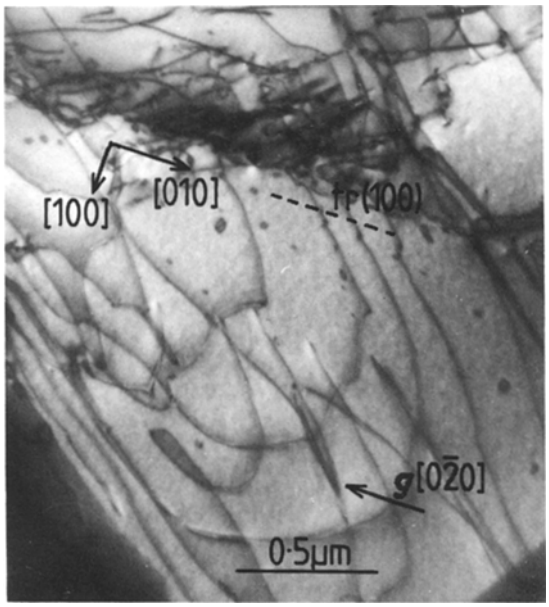

Figure 5 The dislocation structure observed in Zr_3Al deformed 1.3% at 973 K. Bright-field $g = 0\bar{2}0$, beam direction [0 1 0].

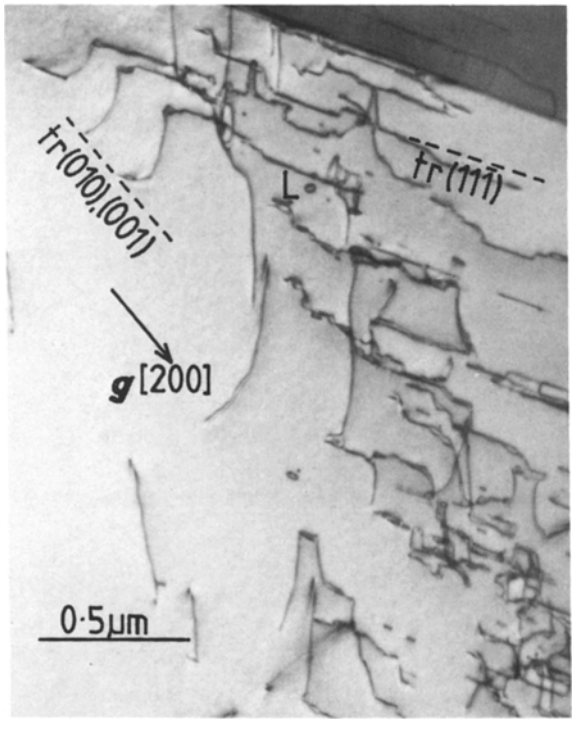

Figure 6 The dislocation structure observed in Zr_3Al deformed 1.2% at 1073 K. Bright-field, beam direction [0 1 1].

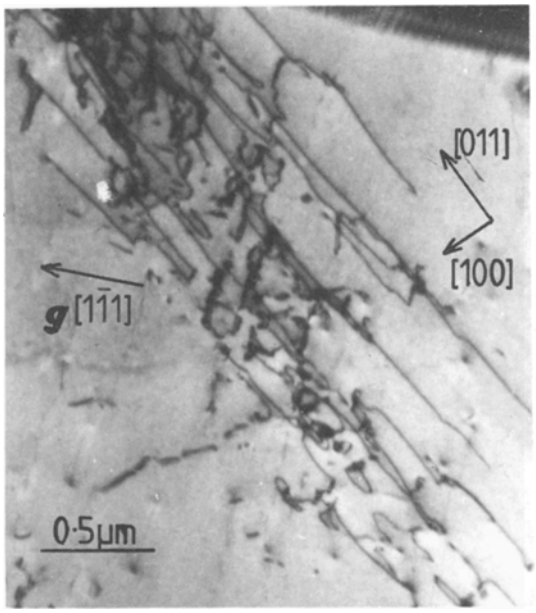

Figure 7 Dislocations observed on both cube and octahedral planes in Zr_3Al deformed 1.2% at 1073 K bright-field, beam direction [0 1 1].

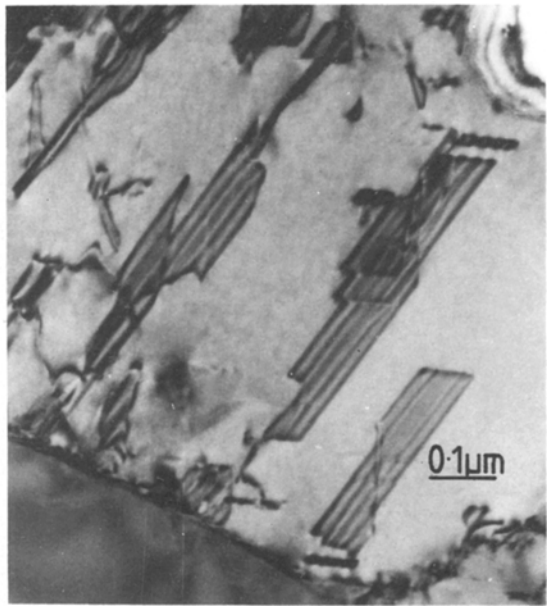

Figure 8 Stacking fault dislocations observed in the titanium alloy T2 deformed 6.5% at 293 K.

particular, the contrast was inconsistent with the following possible types of dissociation scheme

$$\frac{a}{2}\langle 1\,0\,1\rangle \rightarrow \frac{a}{6}\langle \bar{1}\,\bar{2}\,1\rangle + \frac{a}{3}\langle 2\,1\,1\rangle \quad \text{(Fig. 4b)}$$

$$\frac{a}{3}\langle 2\,1\,1\rangle \rightarrow \frac{a}{6}\langle 1\,2\,\bar{1}\rangle + \frac{a}{2}\langle 1\,0\,1\rangle \quad \text{(Fig. 4c)}$$

$$\frac{a}{3}\langle 2\,1\,1\rangle \rightarrow \frac{a}{6}\langle 2\,1\,1\rangle + \frac{a}{6}\langle 1\,2\,\bar{1}\rangle + \frac{a}{6}\langle 1\,\bar{1}\,2\rangle \quad \text{(Fig. 1b)}$$

$$\frac{a}{6}\langle \bar{1}\,1\,1\rangle \rightarrow \frac{a}{6}\langle \bar{1}\,1\,\bar{2}\rangle + \frac{a}{3}\langle 1\,1\,0\rangle \quad \text{(a Frank loop)}$$

The absence of APB dislocations in the binary alloy at 673 K and the relatively small number of S-ISF dislocations in alloys T2 and N1 suggests that the ternary additions increase the stacking fault energy. Measurement of the separation of $a/3\langle 1\,1\,2\rangle$-type partials in alloy N1 at 673 K gave a value of approximately 9 mJ m^{-2} for the $\{1\,1\,1\}\,a/3\langle 1\,1\,2\rangle$ S-ISF energy. This compares with the value of 2 mJ m^{-2} for the binary alloy.

3.4. The observations of planar faults in binary and ternary Zr_3Al-based alloys

Planar faults showing $R = \frac{1}{3}\langle 1\,1\,1\rangle$ S-ISF fringe contrast were observed in both deformed and

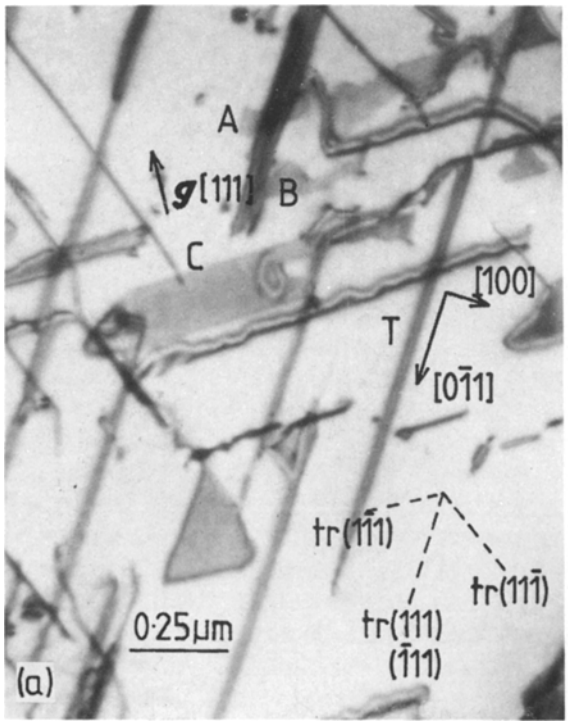

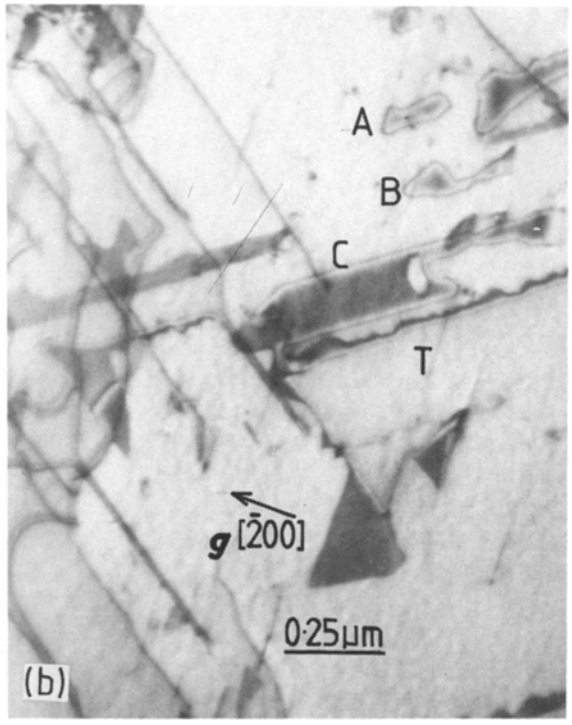

Figure 9 APB and S-ISF dislocations observed in the niobium alloy N1 deformed 1.5% at 673 K. Bright-field, (a) $\boldsymbol{g} = 1\,\bar{1}\,1$; (b) $\boldsymbol{g} = \bar{2}\,0\,0$; beam direction [0 1 1].

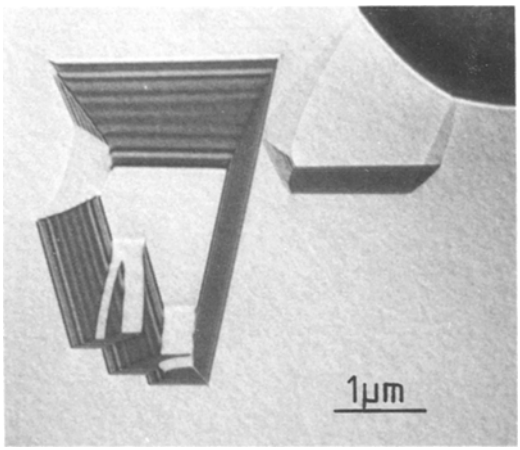

Figure 10 Stacking fault in the niobium alloy N1 heat-treated 24 h at 1160 K.

undeformed Zr_3Al-based alloys of all compositions. In some cases the faults formed a closed ring as shown for the ternary alloy N1 in Fig. 10. Howe *et al.* [6] proposed that such faults are caused by the coalescence of vacancies resulting from the volume contraction which occurs during the peritectoid transformation $Zr + Zr_2Al \rightarrow Zr_3Al$.

4. Conclusions

In binary Zr_3Al-based alloys, deformed at temperatures in the range 273 to 1073 K two types of dislocation dissociation occur depending on the deformation temperature.

(a) For the temperature range 273 to 673 K $a/3\langle 1\,1\,2\rangle$-type partial dislocations bounding S-ISF on $\{1\,1\,1\}$ planes predominate. The $\{1\,1\,1\}\,a/3\langle 1\,1\,2\rangle$ stacking fault energy is approximately $2\,mJ\,m^{-1}$ at 673 K.

(b) For the higher temperature range, 873 to 1073 K, APB separated $a/2\langle 1\,1\,0\rangle$ pairs predominate. Slip occurs on cube planes together with some cross-slip onto octahedral planes. The $\{1\,0\,0\}\,a/2\langle 0\,1\,1\rangle$ APB energy is in the range 30 to $45\,mJ\,m^{-2}$.

Ternary additions of niobium or titanium were found to increase the $\{1\,1\,1\}\,a/3\langle 1\,1\,2\rangle$ stacking fault energy of Zr_3Al with the result that APB and S-ISF dislocations were observed to coexist in approximately equal numbers at 673 K.

Acknowledgements

We gratefully acknowledge Dr E. M. Schulson and Atomic Energy of Canada Ltd, Chalk River Nuclear Laboratories, Ontario, for the provision of the Zr_3Al specimens. We also acknowledge Professor D. W. Pashley, for the provision of research facilities and the SERC for financial support.

References

1. E. M. SCHULSON, lecture at 27th Annual Canadian Metal Physics Conference, Kingston, Ontario, June 8–10, 1977; Atomic Energy of Canada Ltd. Report No. AECL-5843 (1977).
2. E. M. SCHULSON and J. A. ROY, *Acta Metall.* **26** (1978) 29.
3. B. H. KEAR and H. G. F. WILSDORF, *Trans. AIME* **224** (1962) 382.
4. P. A. FLINN, *ibid.* **218** (1960) 145.
5. B. H. KEAR and J. M. OBLAK, *J. Phys.* **35** (1974) C7-35 suppl.
6. L. M. HOWE, M. RAINVILLE and E. M. SCHULSON, *J. Nucl. Mater.* **50** (1974) 139.
7. A. F. GIAMEI, J. M. OBLAK, B. H. KEAR and W. H. RAND, in Procedings of the 29th Annual EMSA, Boston, USA (Claitor, Baton Rouge, 1971) p. 112.
8. S. TAKEUCHI and E. KURAMOTO, *Acta Metall.* **21** (1973) 415.
9. J. W. EDINGTON, "Practical Electron Microscopy in Materials Science", Monograph 3, (Macmillan, London 1975) pp. 20 and 40.
10. S. TAKEUCHI, E. KURAMOTO, T. YAMAMOTO and T. TAOKA, *Jpn. J. Appl. Phys.* **12** (1973) 1486.
11. B. H. KEAR, *Acta Metall.* **12** (1964) 555.
12. S. M. L. SHASTRY and B. RAMASWANY, *Phil. Mag.* **33** (1976) 375.
13. S. LIANG and D. P. POPE, *Acta Metall.* **25** (1977) 485.
14. P. VEYSSIÈRE, J. DOUIN and P. BEAUCHAMP, *Phil. Mag. A* **51** (1985) 469.
15. K. ENAMI and S. NENNO, *J. Phys. Soc. Jpn.* **25** (1968) 1517.
16. J. M. OBLKAK and W. H. RAND, in Proceedings of the 31st Annual EMSA, New Orleans (Claitor, Baton Rouge, 1973) p. 174.
17. L. YE POPOV, I. V. TERESHKO, L. K. GORENKO, N. A. KONEVA, E. V. KOZLOV and T.A. KOVALEVSKAYS, *Phys. Met. Metall.* **35** (1973) 409.
18. R. J. TAUNT and B. RALPH, *Phil. Mag.* **30** (1974) 1379.
19. K. SUZUKI, M. ICHIHARA and S. TAKEUCHI, *Acta Metall.* **27** (1979) 193.
20. K. SUZUKI, E. KURAMOTO, S. TAKEUCHI and M. ICHIHARA, *Jpn. J. Appl. Phys.* **16** (1977) 919.

Received 10 September
and accepted 11 October 1985